The cylindrical container (150 mm O.D. and 57 mm height) allows simultaneous irradiation of 4 cylindrical sample holders (50 mm O.D and 19 mm height), also made of stainless steel. A Pt100 thermocouple which goes from the container to the heating device controls the temperature inside the container. The cylindrical container is shown schematically on Figure 3. The time needed to reach a temperature of 200 ^{o}C is about 90 minutes. Further improvements, which will result in a new cylindrical container, will permit simultaneous irradiation of 8 cylindrical sample holders and 6 encapsulated glass ampoules (50 mm O.D and 250 mm height).

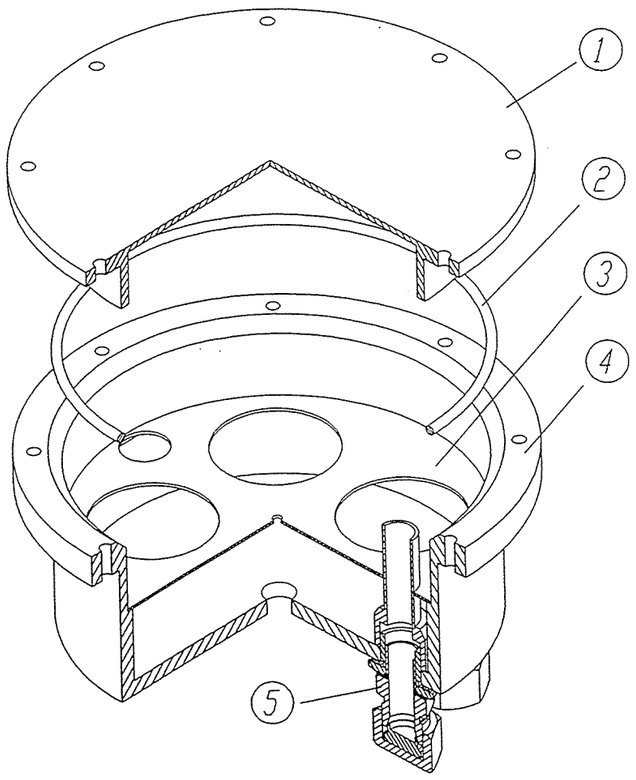

Figure 3: General view of the container: 1.- Lid. 2.- O-Ring. 3.- Intermediate plate. 4.- Frame. 5.- Hosepipe connector.

PART III

PRE-IRRADIATION CHARACTERISTICS OF TWO SALT FORMATIONS

GEOCHEMICAL AND PETROSTRUCTURAL CHARACTERIZATION OF AN EXAMPLE OF BEDDED SALT: POTASAS DEL LLOBREGAT SAMPLES

C.de las Cuevas, L.Miralles, J.García Veigas, P.Teixidor, J.J.Pueyo

ABSTRACT

Geochemical and petrostructural characterization, prior to irradiation experiments, has been performed in samples from the Lower Salt Unit of the Catalonian Potash Basin (Potasas del Llobregat mine). The investigations comprised both fluid (gas and brine analyses) and mineral phases. The rock salt studied is a polycrystalline rock in which halite is the major mineral (around 90 %), the second mineral phase in importance is anhydrite and the rest of mineral phases (quartz, clay minerals, magnesite and celestite) is scarce (below 1%). Neither polyhalite nor any other hydrated mineral was found. The grain size of the halite crystals ranges between 1 mm and 2 cm. The chemical analyses show low magnesium and potassium contents, in contrast to what is found in the Asse mine rock salt (north european Zechstein basin). The water content in the samples studied is as average 0.32 % weight, ranging between 0.04 and 1.00 %. Water is present in form of interstitial (intergranular) brine and as intragranular fluid inclusions. The fluid inclusions contain magnesium (1.15 mol/l) and potassium (0.31 mol/l). The most abundant gas is O_2. Small quantities of CO_2 and traces of CH_4 are also found. At temperatures above 100°C, additional CH_4 is released from the thermal decomposition of organic matter.

1. INTRODUCTION

Radiation damage, which is expected to develop in the rock salt around radioactive wastes, changes the physico-chemical properties of the surrounding rock. Since the rock salt is expected to act as a natural barrier in the case of radioactive waste disposal in salt formations, the properties of the starting material of different salt formations have to be known in order to predict their response to the effect of heat and gamma radiation. Besides thermomechanical perturbation of the rock salt, gas release and water migration are enhanced by the high temperatures and thermal gradients. Moreover, irradiation is responsible for the generation of radiation-induced defects in the halite crystals and for the production of radiolytical gases.

In order to fulfil the objectives of the Spanish research and development program on radiactive waste disposal in salt formations, a preliminary sampling survey was performed in the Potasas del Llobregat potash mine, located in the area of Sallent-Balsareny; Catalonian Potash Basin (north eastern Spain). Bedded salt, with an average thickness of about 300 m is present in that basin. The saline body is divided into a lower salt unit, a potash seam and an upper salt unit (Busquets et al., 1985). Detailed geochemical and petrostructural characterization was performed on the Lower Salt Unit samples, which were chosen to be one of the starting materials for the irradiation experiments performed in the frame of the HAW project. The investigations comprised both the fluid phase (gas and brine analyses) and the mineral phases of the rock salt.

2. METHODOLOGY

2.1 Sampling

Sampling was performed in the Lower Salt Unit, on the mine 323 m level. The samples studied were gained from test cores using flushing air as drilling fluid. A total of 12 horizontal boreholes of 86 mm diameter and 6 m length were drilled. Six boreholes were drilled in an impure salt lower horizon (dark coloured) and the rest in a pure salt upper horizon (white coloured).

2.2 Gas analysis

The content of gas present in the rock salt was measured in laboratory experiments and in *"in situ"* degasification tests.

Laboratory degasification experiments were performed on representative samples of the pure and impure horizon. Immediately after drilling, cores weighing between 1.5 and 2 Kg were stored on site, in borosilicate glasses, which were purged and filled with nitrogen to an overpressure of 0.2-0.3 bar. The natural gas release was quantified after 12 months of storage in the laboratory. Afterwards, those sample holders were purged again in the same manner as previously described, and placed in an oven. Heating took place in three stages up to 60, to 100 and to 150^{o}C respectively. After each degasification period (3 months at constant temperature), gases were analyzed.

"In situ" degasification tests have been carried out in three boreholes drilled in the lower salt horizon, which were sealed with gastight stainless steel packers. Each packer consists of a 70 cm long tube, with a viton seal which is mechanically expanded and pressed against the borehole wall. The parts of the packer that are in contact with the borehole atmosphere are coated with a teflon cap in order to avoid corrosion. The teflon cap has a 10 mm hole, through which a teflon tube passes through the packer. The tube is closed at the gallery wall end with a gastight valve. After sealing the boreholes with the packers, the boreholes were purged and filled with nitrogen to an overpressure of 0.6 bar. Gas sampling was carried out by allowing the gas to flow directly into the sampling bags (Plastigas, Linde). After sampling, the boreholes were refilled with nitrogen. The gas sampling for each borehole, was carried out 7, 14, 24 and 39 months after borehole sealing.

Analytic determination of the gas content was carried out by Gas Chromatography. Gas samples were extracted from the glass containers and sample bags through a septum from a gastight syringe. Quantification of the gaseous components was performed through peak area integration using the external standard method. Samples and standards were injected repeatedly until less than 5% dispersion in the area measurement was observed. The analytical conditions were:

For H_2 and O_2 : Molecular Sieve 5A 80/100 mesh, 3m 1/8" OD; 60^{o}C hold; Carrier gas: Ar, Detector: Thermal Conductivity (TCD).
For CO_2 and light hydrocarbons: Porapak Q 50/80 mesh, 4m 1/4" OD; 120^{o}C hold; Carrier gas: He, Detector: Thermal Conductivity (TCD).

2.3 Water content determination

Water content was determined by Thermogravimetry, since this technique allows to quantify and discern the types of water present in the rock salt. A sample with a grain size of 2 to 3 mm, and weighing 1 g was taken for the analysis. The working conditions were as follows: temperature interval from 20 to 450^{o}C, heating rate of 5^{o}C/min and atmosphere of argon.

2.4 Brine composition determination

The determination of brine composition was performed by X-Ray microanalysis (SEM-EDS) on fluid inclusions. A more detailed description of this method can be found in Ayora *et al.*(1994). Rock salt specimens containing primary structures with fluid inclusions (hopper crystals) were selected, and slices about 1 cm^2 surface and 1 mm thickness were cut with a low speed saw. These slices were polished on both sides, using alumina powder of 0.3 mm in the last polishing stage.

The slice and four droplets of standard solutions were introduced into a sample holder. The holder was immersed in liquid N_2, placed in a lateral chamber of a Scanning Electron Microscope (SEM) and placed on a cryostage at -170°C. The slice was broken inside the chamber and a flat cross section of halite containing a large number of frozen fluid inclusions was obtained. To prevent electric charging the whole sample assemblage was coated with aluminium. Finally, the sample assemblage was placed in the central chamber of the SEM at -180°C.

During the analysis of the standard solutions and fluid inclusions, the X-Rays emitted were captured by a solid state Si (Li) crystal analyzer and converted into a conventional Energy Dispersive Spectrum (EDS). The working conditions were established at 15 kV, 1.5 nA of beam current and 200 seconds of counting time. The microanalysis was carried out for several electrolytes (Cl^-, SO_4^{2-}, Na^+, K^+, Mg^{2+} and Ca^{2+}). Quantitative analysis of the elements is based on the peak-to-background ratio of each EDS peak. The relative analytical error was in all cases lower than 10 %. Detection limits were established for each element. Ca^{2+}, K^+ and SO_4^{2-} had detection limits lower than 0.05 M, whereas those of Mg^{2+} and Na^+ were 0.35 and 0.55 M respectively.

Internal consistency of results was checked by the charge balance (CB) $[Cl^-]+2[SO_4^{2-}]/[Na^+]+[K^+]+2[Mg^{2+}]$. The saturation index (IS) with regard to halite (log $[a_{Na} * a_{Cl}/K_{halite}]$), the host mineral, was used to check the external consistency of the results. In ideal conditions CB equals 1 and IS equals 0. Charge unbalances and saturation indexes lower than +/- 0.2 were interpreted as falling within the range of the analytical error, and therefore those results were considered reliable.

2.5 Chemical analysis of rock salt

Geochemical characterization was performed on 25g of milled salt by analyzing major components such as, Cl, SO_4 and Ca, as well as trace elements which are characteristics in rock salt, such as Mg, K, Sr and Br. Except for bromine, which has been determined by XRF (X-Ray Fluorescence), chemical analysis have been performed after dilution of the sample in distilled water. Cl was determined by volumetry (Mohr method), SO_4 was determined by ICP-AES (Inductively Coupled Plasma Atomic Emission Spectroscopy), K by AES (Atomic Emission Spectroscopy) and Mg, Ca and Sr by AAS (Atomic Absorption Spectroscopy). The insoluble fraction was determined gravimetrically, and the mineral phases present in this fraction were identified by XRD (X-Ray Diffraction) using the oriented aggregates technique.

2.6 Petrostructural characterization

Petrographic observations as well as fabric characterization were perfomed on thin sections by transmitted light microscopy. Low speed sawing and grinding techniques were applied to the production of thin sections in order to avoid damage induced by sample manipulation. The surface obtained by a longitudinal cut of the core was ground with silicon carbide paper of 600, 1000 and 1200 grit (DIN-norm) and polished with diamond powder of 3 µm using an automatic grinder-polisher wheel (Motopol TM, Buehler). Evaporating oil (Shell type S-4919) was used as cooling fluid. These polished surfaces were attached to a glass with a two-component glue (Araldite D + Hardener HY 956) and afterwards sawn to a thickness of 1 mm by a low speed wire saw (Well type 6234). The other side of the sample, which was not attached to the glass, was ground and polished again following the same procedure to a thickness of around 200 µm.

Images of the thin sections were obtained with a video camera adapted to a stereomicroscope (Wild M5A) and afterwards treated by an image analyzer. Differentiation between halite and birefringent minerals was achieved under crossed-polarized light. The grains of the halite fraction were then individualized and converted into a binary image, on which the measurements were performed. Examples of the binary images of samples 3149 and 3143 can be seen in Figures 1 and 2.

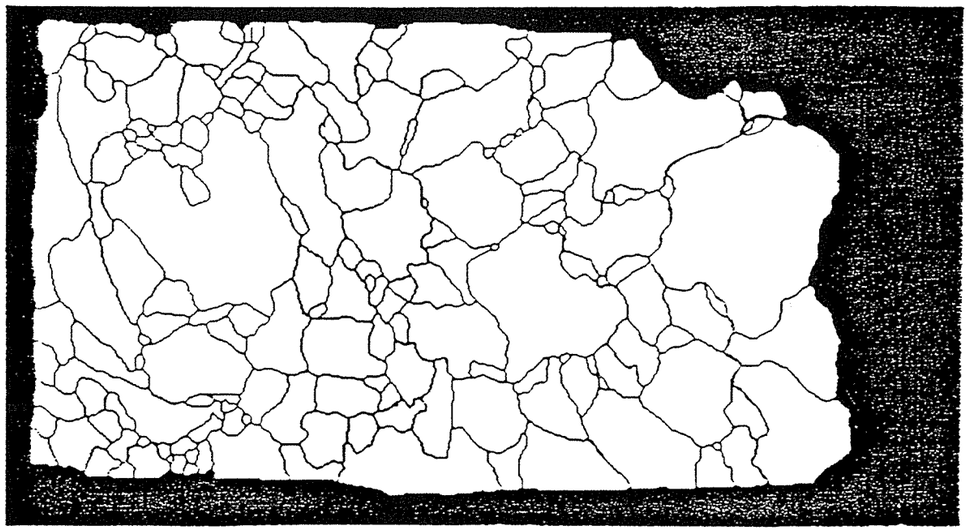

Figure 1: Binary image of sample 3149 (long axis of the sample is 4 cm)

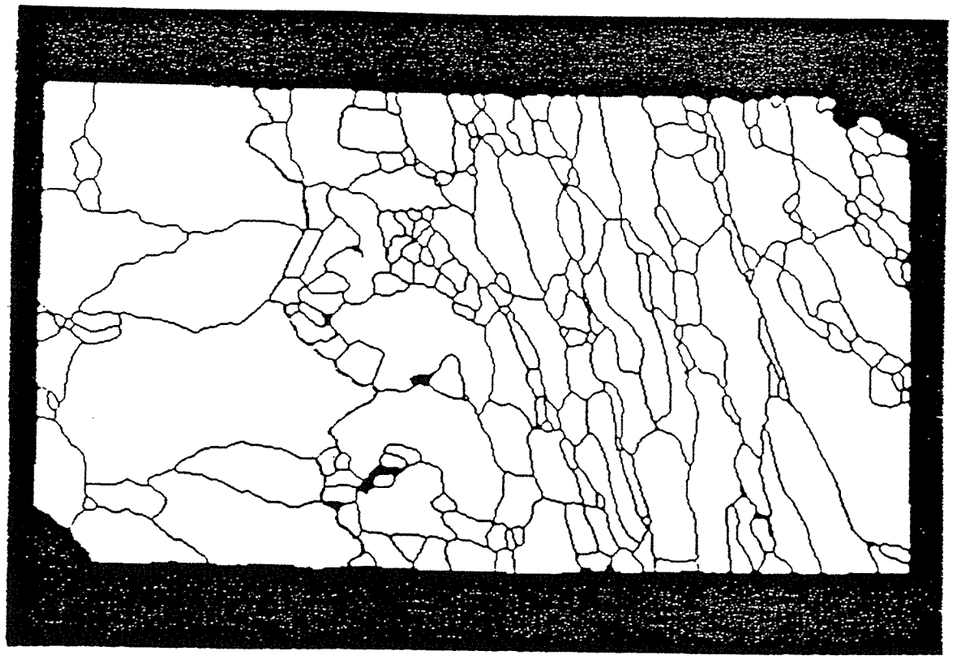

Figure 2: Binary image of sample 3143 (long axis of the sample is 4 cm)

3. RESULTS

3.1 Gas content

The most abundant primary gas present in the rock salt is O_2, followed by CO_2 and CH_4. This was confirmed by both the laboratory experiments at room temperature and the *"in situ"* tests. Moreover, H_2, C_2H_6 and C_3H_8 were also found as traces in the sealed boreholes. The temporal evolution of the concentrations of the different gases within one of these boreholes is plotted in Figure 3. Since gas inflow from the salt formation into the borehole is directly related to the gas content and to the permeability of the rock salt, it seems that during the first year the rapid increase in the gas content could be explained by the degasification of the altered zone close to the borehole (enhanced permeability). After a year, the lower gas fluxes into the borehole could be explained by gas migration from the unaltered rock salt.

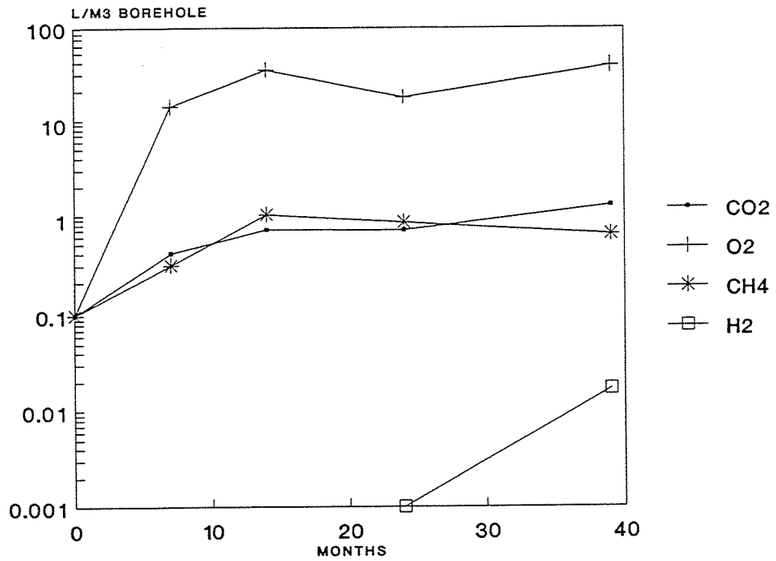

Figure 3: Temporal evolution of gas concentration in one of the sealed boreholes

Table 1 shows the results obtained for laboratory degasification at room temperature, together with the mineral composition. Rock salt rich in impurities tends to exhibit higher contents in CO_2 than pure rock salt. CH_4 is only detected in impure rock salt. There are some discrepancies between laboratory degasification experiments and the *"in situ"* test, regarding the ratios between the concentration of gases: In laboratory experiments the ratios O_2/CO_2, O_2/CH_4 and CO_2/CH_4 are significantly higher than in the *"in situ"* tests.

Table 1: Laboratory degasification test at room temperature.

Sample	O_2	CO_2	CH_4	Clay	NaCl	$CaSO_4$
1122	763.8	1.9	tr	1.37	94.51	4.12
1128	652.4	2.3	tr	0.82	90.22	8.96
1135	773.5	2.7	tr	0.77	85.88	13.35
1216	635.3	1.3	n.d	0.18	97.92	1.90
1221	848.0	2.3	n.d	0.14	98.15	1.71
1227	664.4	1.4	n.d	0.15	98.39	1.46
1233	603.2	1.3	n.d	0.12	97.80	2.08
4116	387.9	3.3	0.12	2.15	85.82	12.03
4123	442.8	4.1	0.11	0.64	88.81	10.55
4132	712.8	5.0	tr	1.37	90.52	8.11
4214	617.4	1.4	n.d	0.27	96.36	3.37
4225	556.8	1.4	n.d	0.09	98.51	1.40
4227	794.3	1.6	n.d	0.13	98.15	1.72
4233	872.2	2.1	n.d	0.17	98.80	1.03

Content of gases expressed as l/m^3 salt. Mineralogical composition expressed in %.
tr: trace (around 0.01 l/m^3 salt) n.d= not detected.

Table 2: Laboratory degasification test at 60°C.

Sample	O_2	CO_2	CH_4	Clay	NaCl	$CaSO_4$
1117	207.3	6.2	tr	0.72	91.69	7.59
1122	280.1	4.1	n.d	1.37	94.51	4.12
1128	268.9	8.8	tr	0.82	90.22	8.96
1135	298.4	13.6	tr	0.77	85.88	13.35
1216	239.1	1.4	n.d	0.18	97.92	1.90
1221	504.4	2.2	n.d	0.14	98.15	1.71
1227	263.5	1.9	n.d	0.15	98.39	1.46
1233	264.1	2.1	n.d	0.12	97.80	2.08
4116	130.4	19.1	tr	2.15	85.82	12.03
4123	214.0	26.2	tr	0.64	88.81	10.55
4132	272.4	16.8	tr	1.37	90.52	8.11
4214	235.6	2.1	n.d	0.27	96.36	3.37
4225	207.0	1.4	n.d	0.09	98.51	1.40
4227	254.9	1.7	n.d	0.13	98.15	1.72
4233	495.8	2.4	n.d	0.17	98.80	1.03

Content of gases expressed as l/m^3 salt. Mineralogical composition expressed in %.
tr: trace (around 0.01 l/m^3 salt) n.d= not detected.

Table 3: Laboratory degasification test at 100°C.

Sample	O_2	CO_2	CH_4	Clay	NaCl	$CaSO_4$
1117	787.3	8.3	tr	0.72	91.69	7.59
1122	1054.0	4.2	tr	1.37	94.51	4.12
1128	978.9	5.4	tr	0.82	90.22	8.96
1135	960.6	5.9	tr	0.77	85.88	13.36
1216	776.7	2.3	n.d	0.18	97.92	1.90
1221	981.5	3.1	n.d	0.14	98.15	1.71
1227	775.7	2.7	n.d	0.15	98.39	1.46
1233	1092.0	2.6	n.d	0.12	97.80	2.08
4116	703.8	21.3	tr	2.15	85.82	12.03
4123	975.6	14.0	tr	0.64	88.81	10.55
4132	1182.3	7.6	tr	1.37	90.52	8.11
4214	813.3	3.4	n.d	0.27	96.36	3.37
4225	767.6	2.3	n.d	0.09	98.51	1.40
4227	802.9	2.6	n.d	0.13	98.15	1.72
4233	1171.6	3.4	n.d	0.17	98.80	1.03

Content of gases expressed as l/m^3 salt. Mineralogical composition expressed in %.
tr: trace (around 0.01 l/m^3 salt) n.d= not detected.

Table 4: Laboratory degasification test at 150°C.

Sample	O_2	CO_2	CH_4	Clay	NaCl	$CaSO_4$
1117	761.6	2.1	0.50	0.72	91.69	7.59
1122	974.7	4.8	3.30	1.37	94.51	4.12
1128	816.6	4.8	6.90	0.82	90.22	8.96
1135	822.6	3.0	0.70	0.77	85.88	13.35
1216	685.3	3.1	tr	0.18	97.92	1.90
1221	1080.0	4.2	n.d	0.14	98.15	1.71
1227	756.4	4.4	0.90	0.15	98.39	1.46
1233	557.4	3.7	0.80	0.12	97.80	2.08
4116	686.4	1.8	0.30	2.15	85.82	12.03
4123	712.9	2.9	0.50	0.64	88.81	10.55
4132	1168.7	2.2	1.10	1.37	90.52	8.11
4225	630.5	5.3	0.40	0.27	96.36	3.37
4227	718.9	3.7	0.30	0.13	98.15	1.72
4223	864.7	5.2	n.d	0.17	98.80	1.03

Content of gases expressed as l/m^3 salt. Mineralogical composition expressed in %.
tr: trace (around 0.01 l/m^3 salt) n.d= not detected.

The results of the laboratory degasification experiments at higher temperatures are shown in Tables 2 to 4 (for temperatures of 60, 100 and 150°C respectively). No differences in O_2 content were observed between pure and impure rock salt. The values of O_2 are very low at 60 °C, while they reach a maximum at 100 °C (thrice than at 60 °C) and yield similar values at 150°C. Since the O_2 concentration in the gas phase at 100 °C (after a degasification period of 6 months) is similar to that obtained at room temperature (after 12 months), it can be concluded that the desorption at 100 °C is at least twice as effective.

In contrast, the behaviour of CO_2 depended on whether the rock salt was pure or had visible mineral impurities. For impure rock salt, which had up to four times more CO_2 than pure rock salt, the amounts of CO_2 released reached a maximum at 60 °C and decreased at higher temperatures, while for pure rock salt the maximum was located at 150°C. A possible explanation for this behaviour could be a reaction of CO_2 with some mineral phase.

CH_4 is only present (as trace) in impure rock salt at temperatures up to 100 °C. At 150°C a high increase in the amount of CH_4 is registered because, between 100 and 150°C, the thermal decomposition of organic matter becomes a relevant process.

3.2 Water content

The results of the studied population (n= 175) are displayed as a histogram in Figure 4. Water content data follow the lognormal distribution, as can be deduced from the histogram. The water content ranged from 0.04 to 1.00 wt%, the average weight loss was of 0.32 % and the standard deviation amounted to 0.20 %. In those samples, water is present in form of interstitial (intergranular) brine and in intragranular fluid inclusions. The average content in intergranular brine was 0.17 % (standard deviation equaled 0.14%) whereas the average content as fluid inclusions was 0.15 % (standard deviation equaled 0.08%). A representative thermogram of the salt studied is shown in Figure 5. In this figure two curves are plotted, one of them gives the variation of temperature with time and the other gives the loss of mass with time. Intergranular brine was liberated up to 120 °C, while fluid inclusions bigger than 30 µm decrepitated between 300 and 350 °C (Mosler, 1990). The last mass loss registered, due to decrepitation of smaller fluid inclusions, took place at 400 °C.

Rock salt rich in impurities had higher amounts of intergranular water than pure rock salt. It seems that clay-anhydrite bearing rock salt would have higher porosity resulting in better entrapment of the brine. Intragranular fluid inclusions are related to the presence of hopper crystals. Comparing these samples with Asse rock salt, Potasas del Llobregat samples

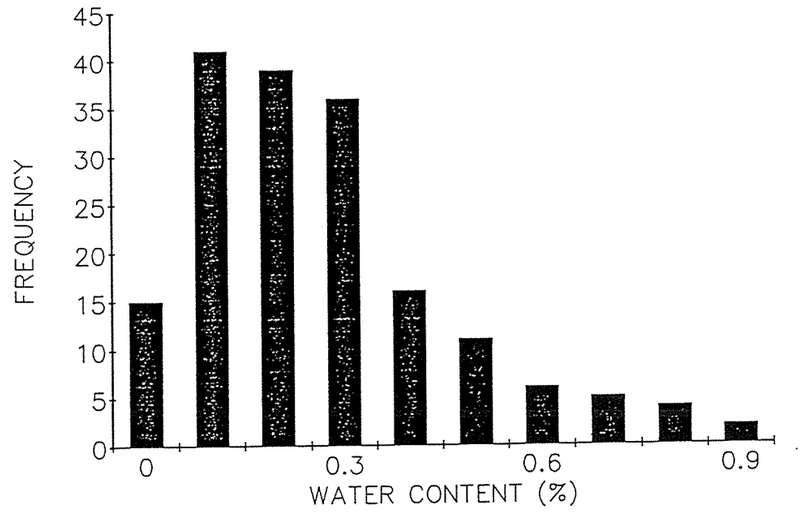

Figure 4: Histogram of the total water content of Potasas del Llobregat samples.

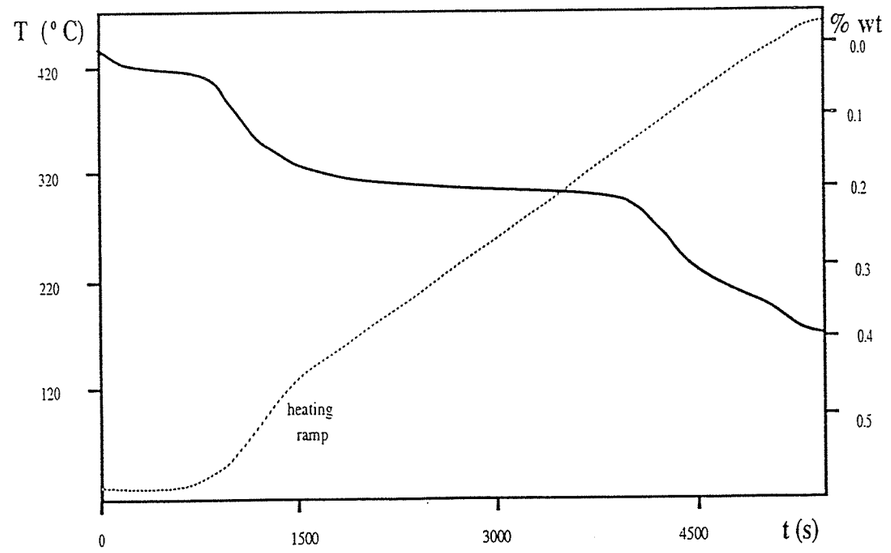

Figure 5: Representative thermogram of Potasas del Llobregat samples.

Table 5: Chemical composition of fluid inclusions

Sample	Na^+	Mg^{2+}	K^+	SO_4^{2-}	Cl^-	CB	IS
41281a	2.59	1.43	0.30	0.05	5.81	0.97	-0.05
41281b	3.20	1.13	0.28	0.08	5.96	0.94	0.03
41281c	2.87	0.90	0.30	0.10	0.16	0.80	-0.07
41281d	2.77	1.03	0.31	0.07	5.76	0.87	-0.14
41281e	2.63	0.93	0.31	0.01	5.98	0.86	-0.17
41281f	2.91	1.27	0.42	0.08	5.98	0.83	0.02
41281g	3.05	1.27	0.29	0.13	6.10	0.92	0.08
41281h	2.87	0.83	0.41	0.09	5.91	0.81	-0.14
41232a	2.58	1.21	0.35	0.10	5.85	0.88	-0.11
41232b	2.68	1.15	0.35	0.06	5.93	0.88	-0.09
41232c	2.77	1.18	0.24	0.05	5.94	0.89	-0.06
41232d	2.92	1.09	0.35	0.05	6.22	0.86	0.01
41232e	2.49	1.04	0.21	0.09	5.77	0.80	-0.21
41232f	3.02	1.32	0.28	0.04	5.74	1.02	0.01
41232g	2.87	1.07	0.33	0.07	6.04	0.86	-0.04
41091a	3.20	1.96	0.30	0.12	6.60	0.80	0.12
41091b	3.04	1.01	0.28	0.03	6.38	0.83	0.03
41091c	3.32	1.13	0.27	0.05	6.15	0.93	0.09
41091d	2.77	1.11	0.21	0.08	6.35	0.80	-0.01
41311a	2.85	1.16	0.38	0.08	6.42	0.84	0.06
41311b	2.96	0.92	0.33	0.04	5.76	0.88	-0.13
41111a	2.84	1.18	0.35	0.04	6.26	0.87	0.02
41111b	2.75	1.04	0.42	0.07	6.23	0.82	-0.04
41111c	3.21	1.35	0.17	0.05	6.35	0.94	0.18
41111d	3.49	0.92	0.32	0.06	6.12	0.91	0.06
41111e	3.35	1.21	0.39	0.11	6.02	0.98	0.13

Note: Ionic concentrations expressed in mol/litre. Variable CB stands for charge balance. Variable SI stands for saturation index.

can be considered as water-rich rock salt. This difference can be attributed to the low degree of tectonism, since Potasas del Llobregat samples are full of primary structures and Asse salt has undergone recrystallization processes (Gies et al., 1994).

3.3 Brine composition

The results of the analyses considered reliable are given in Table 5. The brine had an average composition of 2.92 mol/l in Na^+, 1.15 mol/l in Mg^{2+}, 0.31 mol/l in K^+, 0.07 mol/l in SO_4^{2-} and 6.07 mol/l in Cl^-. The Ca^{2+} content in the brine was lower than the detection limit of the cryo-SEM-EDS methodology. Comparison of the results with those reported by Nishri et al. (1988) from seepages at level 800 of the Asse mine shows that the Cl^- and SO_4^{2-} contents in the Potasas del Llobregat brines are similar to those in Asse, the Na^+ content is higher and K^+ and Mg^{2+} are depleted in Potasas del Llobregat in relation to those from Asse.

After halite precipitation, the concentration of Na^+ in residual brines arising from the evaporation of seawater decreases with increasing salinity. Moreover, the Mg^{2+} content in the brine is an indicator of the degree of evaporation of a basin, provided no magnesium-bearing minerals precipitated (McCaffrey et al., 1987). The composition of Potasas del Llobregat brines corresponds to that expected from the evaporation of seawater, although the higher contents in Na^+ and the lower contents of Mg^{2+} in those brines suggest a lower degree of seawater evaporation compared to the Asse brines.

3.4 Chemical composition of rock salt

The statistical data (n=121) of the chemical composition are given in Table 6. The analyses performed on this type of rock salt showed low Mg and K contents in contrast to the Asse rock salt. Furthermore, the amount of SO_4, Ca and Sr is scattered due to differential presence of anhydrite and celestite in the samples. Br, Mg and K are more homogeneously distributed, due to the fact that they are not major components in any mineral phase. In some samples, chemical analyses were performed in two aliquots in order to find out whether these elements are present in the crystal lattice of halite or in the brine as constitutive ions. The first aliquot was dry milled and the second one was milled in alcohol which acts as a trap for the brine (Moretto, 1988). After having analyzed both aliquots of each sample, a great depletion of K, and Br was observed and in the aliquot milled in alcohol, whereas Mg was totally eliminated. This fact would indicate that Mg is only present in the brine, whereas K and Br would be present both in the brine and in the halite lattice.

Table 6: Chemical Composition of Potasas del Llobregat samples

	RANGE	AVERAGE	ST.DEVIATION
NaCl (%)	73.45-99.50	93.53	5.58
INS (%)	0.12- 1.61	0.52	0.39
SO_4 (%)	0.36-18.50	4.02	3.56
Ca (%)	0.05- 6.94	1.57	1.42
K (ppm)	22-409	127	63
Mg (ppm)	41-485	169	92
Sr (ppm)	27-1231	279	224
Br (ppm)	52-117	60	9

Note: INS stands for Insoluble fraction (basically clay minerals)

3.5 Petrography

Microscopic observations showed that the Potasas del Llobregat samples consisted of halite with anhydrite as main impurity. The rest of the mineral phases (clay minerals, quartz and carbonates) were scarce. The clay fraction was constituted by illite, chlorite (+kaolinite) and interstratified chlorite vermiculite. Neither polyhalite nor other hydrated minerals was found. The grain size of the halite crystals ranged between 1 mm and 2 cm.

The biggest halite crystals were formed by a core, made of one or more fragments of primary structures such as pyramidal hopper crystals, and an outer rim of hyaline salt. These hopper crystals (skeletal cubes with depressed faces resulting from fast growth along the edges of an embryo cube) are characterized by a great number of liquid inclusions in the form of oriented negative crystals, which record the directions of quick crystal growth. Hopper crystals form in the brine-air interphase (Dellwig, 1955). The overgrowth of hyaline salt (free of fluid inclusions) is in crystallographic continuity with the fragments of hopper crystals which may have undergone a dissolution process before reaching equilibrium and then acted as nuclei for the hyaline salt.

The rest of the halite grains consisted of hyaline salt of smaller size (around 2 mm average). These crystals have grown on the bottom of the basin where they precipitated under oversaturated conditions. These hyaline crystals, considered by many authors as diagenetic salt grains (Shearman, 1970), usually infill the cavities left over between the already existing bigger grains, reducing the initial porosity.

Subsequent phenomena of dissolution of the more unstable grains have taken place during diagenesis, causing temporary supersaturation on the surface of the more stable grains,

and favouring their enlargement. Nevertheless, the area affected by these phenomena is not large since most of the primary structures are well preserved.

The anhydrite crystals are mainly located at the halite-halite grain boundaries although they can occasionally be found inside the halite grains. The size of anhydrite crystals ranges from 200 to a few micrometers and they are predominantly elongated along the crystallographic c-axis.

Decoration of the samples by gamma irradiation reveals that most of the hyaline halite grains show a well developed subgrain structure with a mean subgrain size of 150 μm, which indicates that grains have undergone some stress after their precipitation. Moreover, different sets of planar arrays (slip-bands) are overprinted on the previous subgrain structures.

3.6 Fabric Analysis

The fabric of the Potasas del Llobregat salt was studied. The term fabric includes the complete spatial and geometrical configuration of all those components that make up the rock salt and their relation to each other. First, the size (area), shape (circular factor, elongation factor and rugosity factor) and grain arrangement (orientation of the grains to a known direction, known as orientation angle) parameters were quantified. Afterwards, the data were statistically treated (see table 7). The obtained results should be considered as a preliminary approximation, since the analysis was performed in 2-D and also because the shape factors are only an approximation of the real grain shape. Nevertheless, they are included because the mechanical strength of rock salt depends on fabric characteristics (Gutzon-Larsen and Lagoni, 1984).

The frequency distribution of the grain area is of lognormal type, as shown in figure 6, in which the major part of the grains (in average 80 %) belongs to the fine sized fraction. According to the measured grain area, grains are grouped into three categories: fine sized grains (area < 0.1 cm^2), medium sized grains (area between 0.1 cm^2 and 0.3cm^2) and large sized grains (area > 0.3 cm^2). Usually, the large sized grains are the ones which contain primary structures or fragments of them, while the grains of the other two categories consist of hyaline salt.

The shape of the halite grains has been determined by measuring the elongation and circular factor while the degree of intergrowth between halite grains has been determined by computing the rugosity factor.

Table 7: Fabric parameters of the studied rock salt

SAMPLE	Grain Area *	**	***	C.F. mean	s.dev	E.F. mean	s.dev.	R.F. mean	s.dev.	Imp. %
3152B	70	30	0	0.66	0.13	0.56	0.15	0.79	0.10	2.16
3152C	97	3	0	0.68	0.16	0.53	0.15	0.76	0.12	3.08
3149A	85	11	4	0.67	0.15	0.59	0.15	0.77	0.12	4.15
3254B	90	5	5	0.65	0.18	0.54	0.14	0.76	0.11	6.68
3129A	85	13	2	0.70	0.18	0.59	0.15	0.76	0.13	13.85
3129B	95	3	2	0.72	0.18	0.57	0.15	0.75	0.12	10.44
3128B	90	6	4	0.72	0.16	0.60	0.15	0.75	0.13	22.04
3143A	85	13	2	0.65	0.20	0.51	0.17	0.74	0.13	13.27
3143C	95	5	0	0.66	0.18	0.52	0.16	0.78	0.12	7.36
3128A	85	12	3	0.67	0.16	0.58	0.16	0.78	0.12	5.50
3143B	85	12	3	0.66	0.18	0.51	0.17	0.78	0.12	4.89

Note: Grain area expressed as relative frequency. * < 0.1 cm^2; ** 0.1 - 0.3 cm^2; *** > 0.3 cm^2. C.F stands for circular factor. E.F stands for elongation factor. R.F stands for rugosity factor. Imp stands for mineral impurity content

The elongation factor (EF) is defined as the ratio of the minimum diameter to the maximum diameter. The mean values varied from 0.51 to 0.60, indicating that, on average, grains display some elongation with their long axis approximately twice as long as their short axis. Althougth there is no correlation between the elongation factor and grain size, the medium sized grains are the most elongated. In sample 3143, the elongated grains are localized in a band defining a foliation direction and therefore this feature is more evident, while in the rest of the samples the elongated grains are randomly distributed. Figure 7 shows the histogram of the elongation factors of sample 3143, which is of normal type.

The circular factor (CF) is defined according to the following formula: 4π Area/perimeter^2, which means that values close to 1 represent a perfect circle. The mean values obtained for Potasas del Llobregat samples vary from 0.65 to 0.72 showing a small scatter. The circular factor is only valid, when it is assumed that the initial shape is a strictly convex circle (Pannozzo and Hürlimann, 1983). For this reason, the grains of Potasas del Llobregat samples have been interpreted as being closer to an ellipse or a square of convex shape than to a circle. The histogram obtained for sample 3143 is shown in figure 8.

The rugosity factor (RF) is defined as the ratio of the convex perimeter to the perimeter of each grain. The value Rf=1 is given to a round object without indentations. The

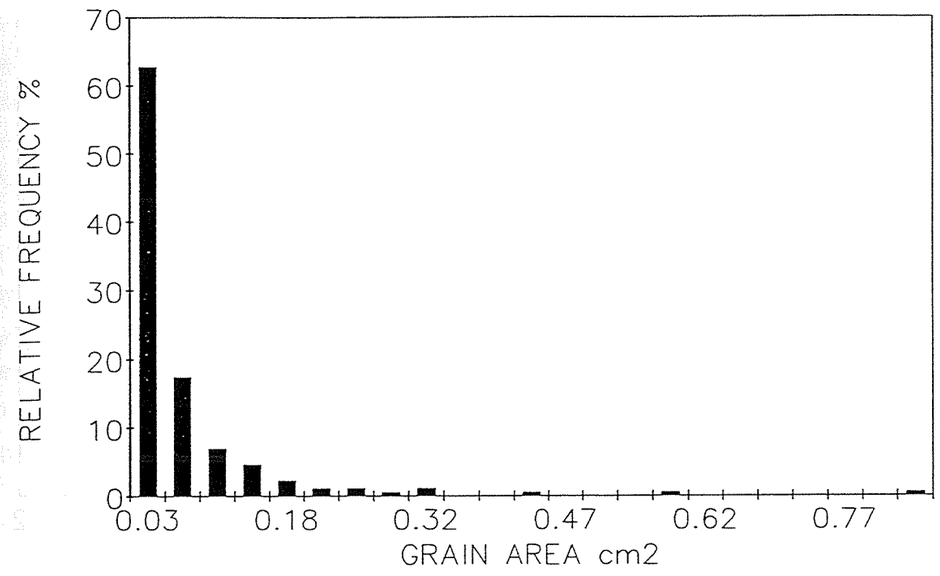

Figure 6: Histogram of the grain area of sample 3143

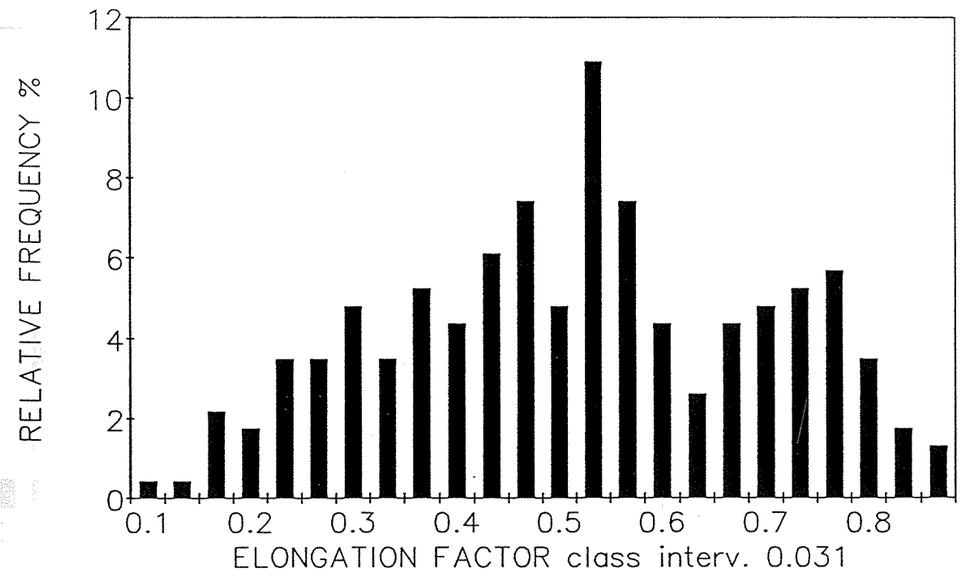

Figure 7: Histogram of the Elongation Factor of sample 3143

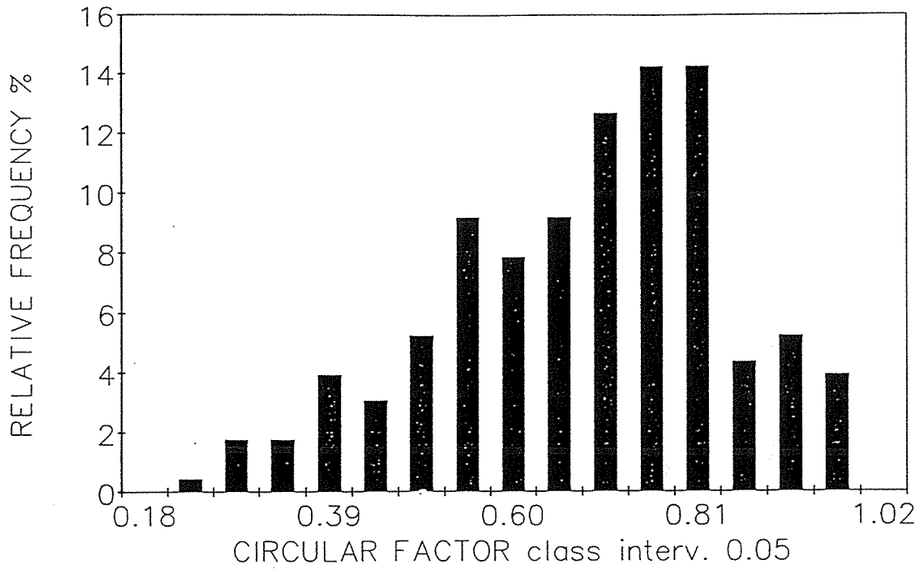

Figure 8: Histogram of the Circular Factor of sample 3143

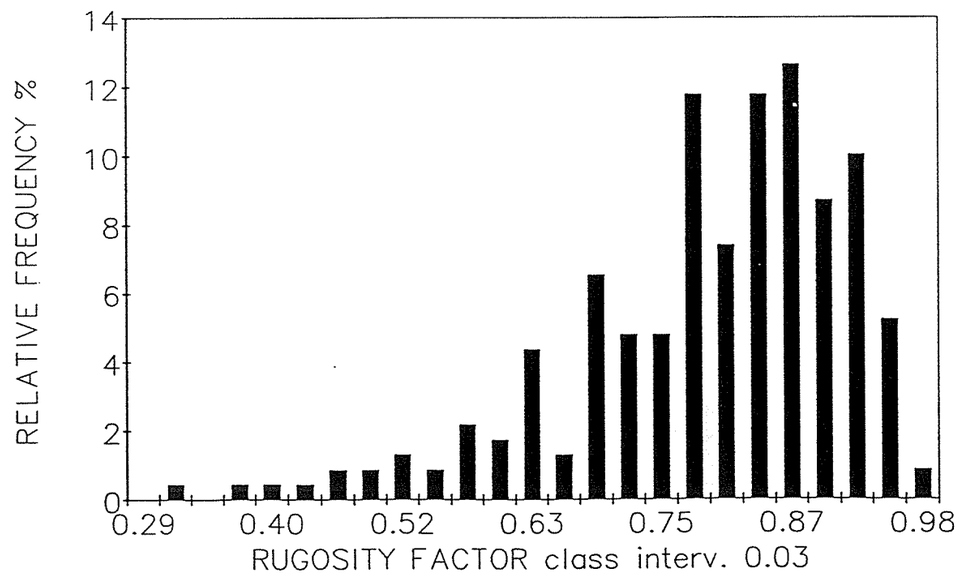

Figure 9: Histogram of the Rugosity Factor of sample 3143

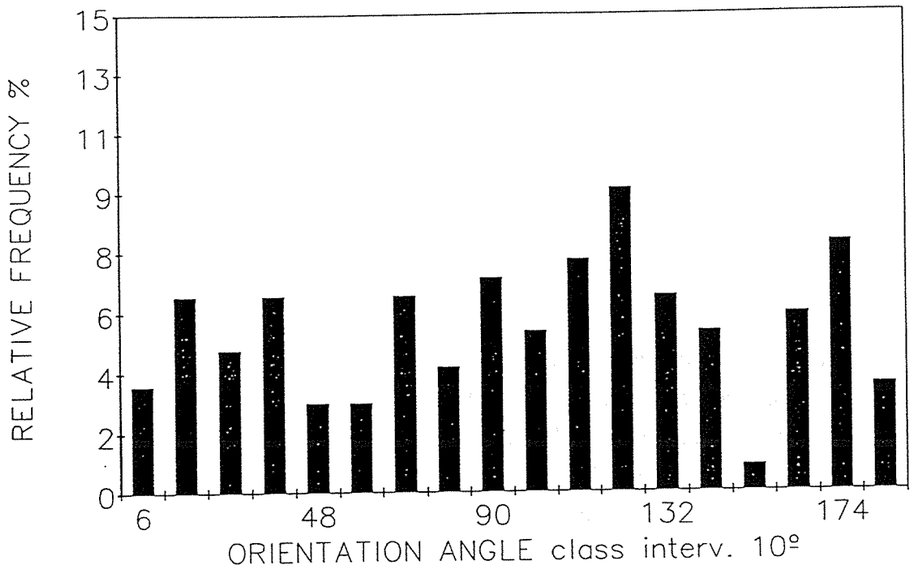

Figure 10: Histogram of the orientation angle of sample 3149

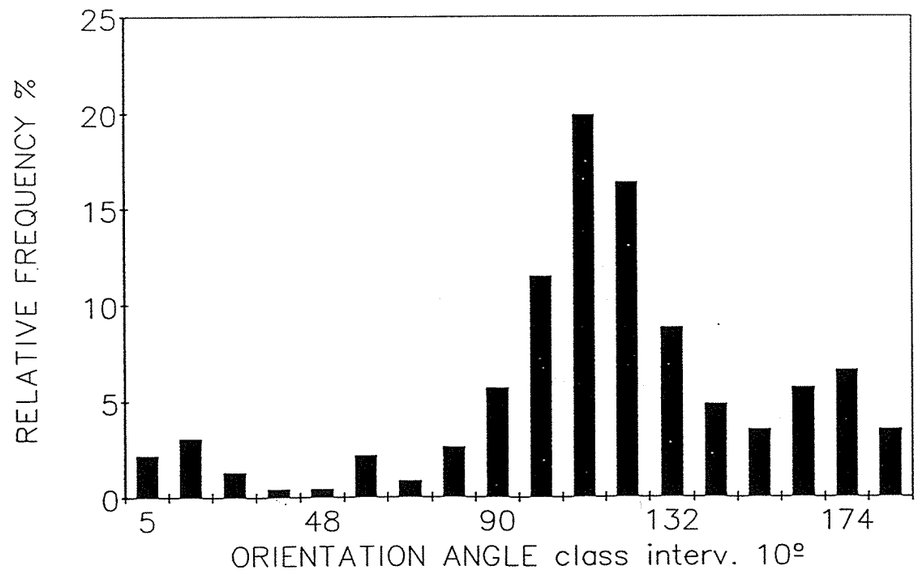

Figure 11: Histogram of the orientation angle of sample 3143

results are also listed in table 7. The mean values range from 0.74 to 0.79, giving numerical information about the convexity-concavity of grain boundaries. There is a positive correlation between the rugosity factor and the grain size. Since the indentations are of the same absolute depth for big and small sized grains, the rugosity factor is lower for the small sized grains. Figure 9 shows the histogram of the rugosity factor of sample 3143.

In order to find out whether there is a preferred form orientation, the angle between the long axis of each grain and the X-axis of the thin section was measured. A frequency distribution of the orientation angles, which are classified in intervals of 10 degrees, was then plotted as a histogram for each sample. Figure 10 shows a histogram of the sample 3149, where the grains are randomly distributed, whereas figure 11 shows the histogram for sample 3143, where a large number of grains show a preferred orientation. In the last case, the morphological directions of grains are grouped in an interval of 40 degrees, defining a foliation direction.

4. CONCLUSIONS

The geochemical and mineralogical characterization of Potasas del Llobregat, as an example of bedded rock salt, prior to irradiation experiments, has been carried out. Two salt facies have been distinguished: rock salt rich in mineralogical impurities (dark salt) and rock salt poor in mineralogical impurities (white salt). Halite is the major mineral (around 90 %), the second mineralogical phase in abundance is anhydrite while the rest of mineral phases (quartz, clay minerals, magnesite and celestite) is scarce (below 1%). Neither polyhalite nor any other hydrated mineral was found.

The chemical analyses show low magnesium and potassium contents in contrast to the Asse mine rock salt (due to the absence of polyhalite), and large variations in the amount of SO_4, Ca and Sr (due to variation in the amounts of anhydrite and celestite in the samples). Br and K are present in the brine as well in the halite lattice, whereas Mg is found only in the brine.

The water content is on average 0.32 % weight, ranging between 0.04 and 1.00 %. Water is present in form of interstitial (intergranular) brine and as intragranular fluid inclusions. In general rock salt rich in mineralogical impurities shows more intergranular water content than pure rock salt. The average content in intergranular brine is 0.17 % whereas the average content in fluid inclusions is 0.15 %. Potasas del Llobregat samples can be considered as water rich rock salt in contrast to Asse rock salt. Moreover, brine

composition in fluid inclusions is similar to that of the Asse brines in Cl^- and SO_4^{2-} contents, althought Na^+ content is higher and K^+ and Mg^{2+} depleted in relation with Asse brines.

The most abundant gas released at room temperature is O_2, as seen in both types of experiment ("*in situ*" and at the laboratory). Small quantities of CO_2 and traces of CH_4 are also found. Rock salt with mineral impurities shows higher contents in CO_2 than pure rock salt and the presence of CH_4. In the *"in situ"* test, the equilibrium inside the borehole has been reached after one year. At the end of the test, small amounts of H_2 were measured in contrast to the laboratory experiments, which could come either from corrosion of the packer or from undetermined sources.

The effect of the temperature, which has been studied only in laboratory experiments, enhances the release of CO_2, and the amounts of O_2 were slightly higher than in room temperature degasification. Rock salt with impurities shows higher contents in CO_2 and of CH_4 than pure rock salt at temperatures up to 100°C. Moreover, there is a high increase in the amount of CH_4 from the thermal decomposition of the organic matter, which starts in the temperature interval between 100 and 150°C.

The grain size of the halite crystals ranges between 1 mm to 2 cm. The biggest halite crystals usually contain one or more fragments of primary structures (hopper crystals) and an outer rim of hyaline salt. The rest of halite grains consist of hyaline salt of minor size (around 2mm average). Most of the hyaline halite grains show a well developed subgrain structure with a mean subgrain size of 150 μm, which indicates that grains have undergone some stress after their precipitation. Moreover, different sets of planar arrays (slip-bands) are also overprinted on the previous subgrain structures. The anhydrite crystals are mainly located at the halite-halite grain boundaries although they can occasionally be found inside the halite grains. The size of anhydrite crystals ranges from 200 to a few micrometers and they are predominantly elongated along the crystallographic c-axis.

The fabric analysis of the rock salt shows that halite grains with areas less than 0.1 cm^2 represent around 80 % of the total amount of grains of the studied samples. Their shape is closer to an ellipse or a square of convex shape than to a circle, and they have some elongation (long axis is approximately twice the short axis) and have a low degree of rugosity. In general, grains are randomly distributed without a preferred shape orientation.

ACKNOWLEDGEMENTS

The work reported here has been performed on behalf of ENRESA under contract No 70.2.3.13.03. We are indebted to Mr. J.M. Grosso from the LIFS for its assisstance at the laboratory.

5. REFERENCES

AYORA, C., GARCIA VEIGAS, J. and PUEYO, J.J., 1994: *"X-ray microanalysis of fluid inclusions and its importance to the geochemical modeling of evaporite basins"* Geochimica et Cosmochimica Acta, **58**, 43-55

BUSQUETS, P., ORTI, F., PUEYO, J.J., RIBA, O., ROSELL, L., SAEZ,A., SALAS, R. and TABERNER, C., 1985: *"Evaporite deposition and diagenesis in the Saline (Potash) Catalan Basin, Upper Eocene"* VI European Regional Meeting IAS, Lleida, Excursion Guide-book: 11-59

DELLWIG, L.F., 1955: *"Origin of Salina salt of Michigan"* Jour. Sed. Petrology, **25**, 83-93

GIES, H., GRESNER, H., HERBERT, H.J., JOCKWER, N. MITTELSTÄDT, R., MÖNIG, J. and NADLER, F., 1994: *"Das HAW-Projekt. Versucheinlagerung hochradioaktiver Strahlenquellen im Salzbergwerk Asse. Stoffbestand und Petrophysik des Steinsalzes im HAW-Feld (Asse, 800-m-Sohle)"* GSF-Bericht 16/94, 186p

GUTZON-LARSEN, J. and LAGONI, P., 1984: *"Zechstein Salt Denmark; Salt Research Project EFP-81, Vol 3 : Fabric Analysis of domal rock salt"* DGU Series C, 1, 100p

MCCAFFREY, M.A., LAZAR, B. and HOLLAND H.D., 1987: *"The evaporation path of seawater and coprecipitation of Br- and K+ with halite"* Jour. Sed. Petrology, **57**, 928-937

MORETTO, R., 1988: *"Observations on the incorporation of trace elements in halite of Oligocene salt beds, Bourg-en-Brese Basin, France"* Geochimica et Cosmochimica Acta, **52**, 2809-2814

MOSLER, H., 1990: *"Gas- und Lösungseinschlüsse im Halitit unter Wärmefeldbedingungen"* Z.Geol.Wiss., **18**, 63-71

NISHRI, A., HERBERT, H.J., JOCKWER, N. and STICHLER, W., 1988: *"The geochemistry of brines and minerals from the Asse Salt Mine, Germany"* Appl.Geoch., **3**, 1-16

SHEARMAN, D.J., 1970: *"Recent halite rock: Baja California, Mexico"* Inst. Mining. Met. Trans., **79**, 155-162

PANNOZZO, R. and HÜRLIMANN, H., 1983: *"A simple method for the quantitative discrimination of convex and convex-concave lines"* Microscopica Acta, **87**, 169-176

SALT OF THE UPPER PERMIAN (ZECHSTEIN-) SALT DIAPIR OF THE ASSE

H. Gies, A. Garcia Celma

ABSTRACT

The Asse salt has many times been used in experiments aimed at a better understanding of the rheological and fluid transport properties of rock salt. In the last decade, it has also repeatedly also been subject of γ-irradiation experiments which have been planned and carried out in order to increase our knowledge of the consequences that radiation and heat will have on the rock salt of prospective radioactive waste repositories. In this frame the Asse rock salt has been used in two different ways, as drilled cores of solid salt, and as mixtures of ground salt of various mineralogical and geochemical composition. This contribution gives a characterization of the salt used in these experiments.

1. GENERAL GEOLOGICAL SITUATION

The Asse salt anticline is part of the subherzynian basin about 30 km north of the Harz mountains. The major rock salt horizon of the Asse is the Staßfurt halite (Na2) which more or less represents the lowermost part of the entire Upper Permian (Zechstein) salt profile in North Germany. It can largely be considered representative also for other sites in the North German Basin, such as Gorleben. The Zechstein (about 250 to 220 my b.p.) is underlain by the lower permian "Rotliegendes" but overlain by the lower triassic "Buntsandstein".

The Staßfurt Hauptsalz / Main Salt (Na2β) generally represents the thickest salt horizon. It consists almost exclusively of anhydritic rock salt (see below), except for its top, and has the more or less same composition and character throughout its entire thickness profile. Fig. 1 shows the stratigraphical sequence at the special position of the HAW-test field in the Asse, which was described in greater detail elsewhere [H. Gies et al., 1994] in the frame

of the HAW-final report. Within the Staßfurt Series the Main Salt is overlain by the Speisesalz (Na2S) horizon.

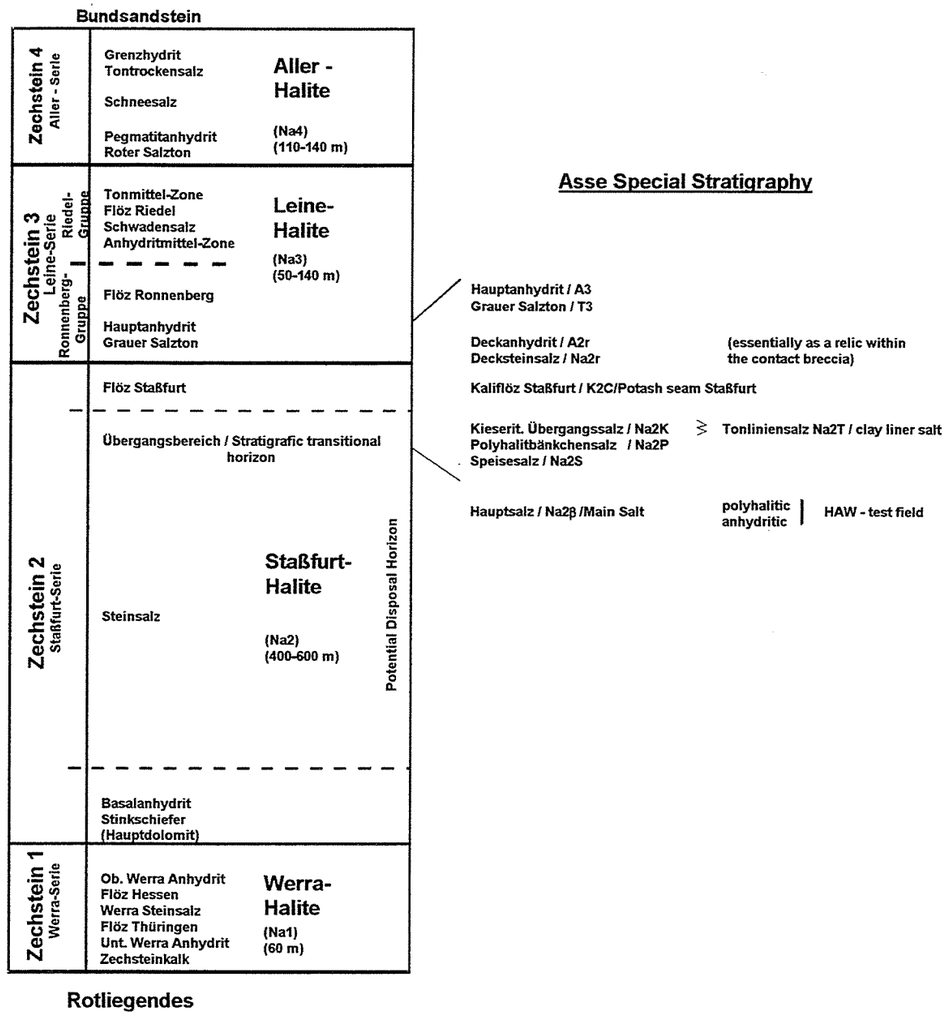

Figure 1: *General stratigraphy of the Upper Permian (Zechstein) in North Germany with special stratigraphy of the uppermost Staßfurt halite/lower Leine series at the Asse*

2. MINERALOGICAL AND GEOCHEMICAL CHARACTERIZATION

The Main salt (Na2β) can be divided into the most abundant (400 to 600 m thick) anhydritic main salt ($Na2\beta_a$) and the less abundant (~ 15 m thick) polyhalitic main salt ($Na2\beta_p$). Salt samples from these two sub-horizons have been used in the laboratory irradiation experiments, either as mixtures of broken salt for radiolytic gas research [Jockwer et al., 1995 (article nr. 13, this volume), Gaudez et al., 1995 (article nr. 14, this volume)], and determination of radiation damage formation [Mönig et al., 1995, article nr. 16, this volume] or as drilling cores of solid salt. In some of the papers in this volume, however, a different sample designation was used [Donker and Garcia Celma, 1995, articles nr. 17 and 18, this volume, Garcia Celma and Donker, 1994], where they were called Borehole anhydritic (Bha) and Borehole polyhalitic (Bhp) salt, respectively.

The mean mineralogical composition of the two sub-horizons was given by Pahl [Pahl, 1988]:

Table 1: *Mean mineralogical composition of the anhydritic Staßfurt main salt and its polyhalitic top*

	anhydritic main salt ($Na2\beta_a$) [% by weight]	polyhalitic main salt ($Na2\beta_p$) [% by weight]
halite	94.6	96.3
anhydrite	4.3	0.8
polyhalite	0.4	2.8
water	0.04	0.18

The quantities of water given here represent the total water comprising the polyhalite crystal water (5.98 % by weight of the polyhalite present) and the interstitial water of the pore spaces. Since all components were determined analytically the difference to 100 % reflects the analytical accuracy. Various clay minerals and magnesite are usually found as trace minerals, mostly around or below their detection limits. Kieserite and sylvite occur, if at all, only in the uppermost Na2 above the Polyhalitbänkchensalz Na2P, closer to the Staßfurt potash seam.

3. MICROSTRUCTURAL CHARACTERIZATION

A direct microstructural characterization of the salt mixtures used in the German irradiation programme was not performed. Previous investigations [Urai et al., 1987] showed that the Asse salt reveals very little internal dislocation structure and indicate low dislocation densities. High internal strain features such as slip bands and kinks band (indicative ôf dislocation glide mechanisms) are almost entirely absent. But these results were gained on Asse Speisesalz, Na2S, a salt that is much more recrystallized due to its high purity than the main salt itself [Spiers et al., 1986, 1988, Peach et al., 1987, Peach, 1991]. This is also expressed by a larger volume of salt showing grain shape fabrics [Gies et al., 1994]. The general applicability of those results seems, therefore, to be limited.

4. PREPARATION AND CHARACTERIZATION OF BROKEN SALT MIXTURE

The salt samples were prepared by mixing salt from two different horizons, in order to have both accessory sulfate minerals present in the salt samples. The final mixture had grain sizes of between 1 and 3 mm. It was split into a large number of subsamples using a sample splitter. In order to confirm that the subsamples had identical compositions five subsamples were chemically analyzed. The compositions found are listed in Table 2.

Table 2: *Mineralogical composition of five rock salt samples to be irradiated and measured (% by weight.)*

	1	2	3	4	5
halite	97,72	97,40	97,66	97,58	98,09
anhydrite	1,80	2,16	1,87	1,94	1,45
polyhalite	0,48	0,44	0,47	0,48	0,46
water	0,042	0,038	0,040	0,037	0,038

The above compositions are considered to be satisfactorily representative for the individual samples that were filled into the ampoules. In total, 160 ampoules each having 300 g of rock salt were prepared, sealed and irradiated in the HFR at Petten (for results see Jockwer et al. [article nr. 13, this volume] and Mönig et al. [article nr. 16, this volume]). As everytime the entire subsample participates in the production of radiolytical gases

The situation, however, is very different when partial samples are being taken for the calorimetric determination of stored energy. In that case, the single sample to be measured weighs only ~ 0.3 g.

The microscopic picture shows very clearly an intergrowth of the halite and sulfate components too close as to allow for a mechanical separation of the minerals (Fig. 2). Likewise, no method is available to take a single specimen having the representative bulk composition.

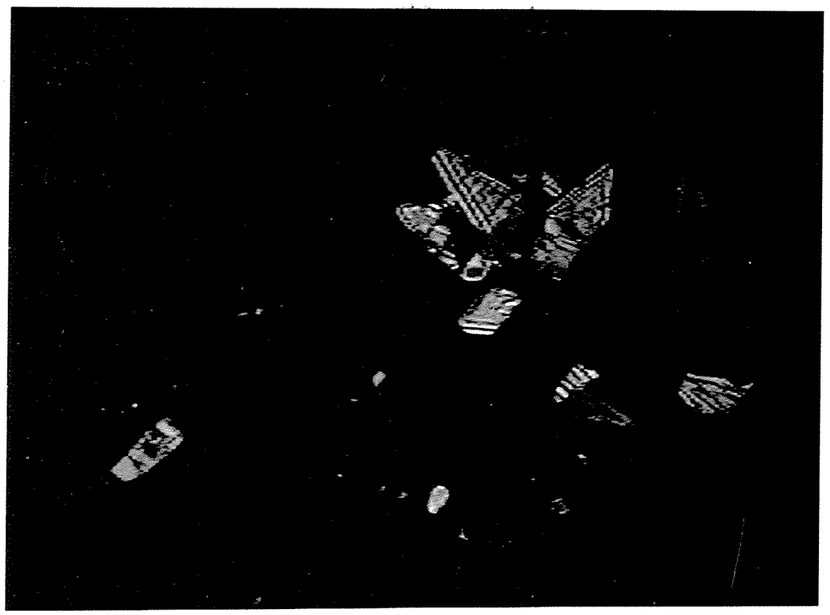

Figure 2a: *Polyhalite and anhydrite crystals in halite (black). (The grain sizes shown here are the coarser ones; a lot of the sulfate portion of the rock salt is represented by very fine grained particles of a few microns). long edge = 1 mm; Nicols +*

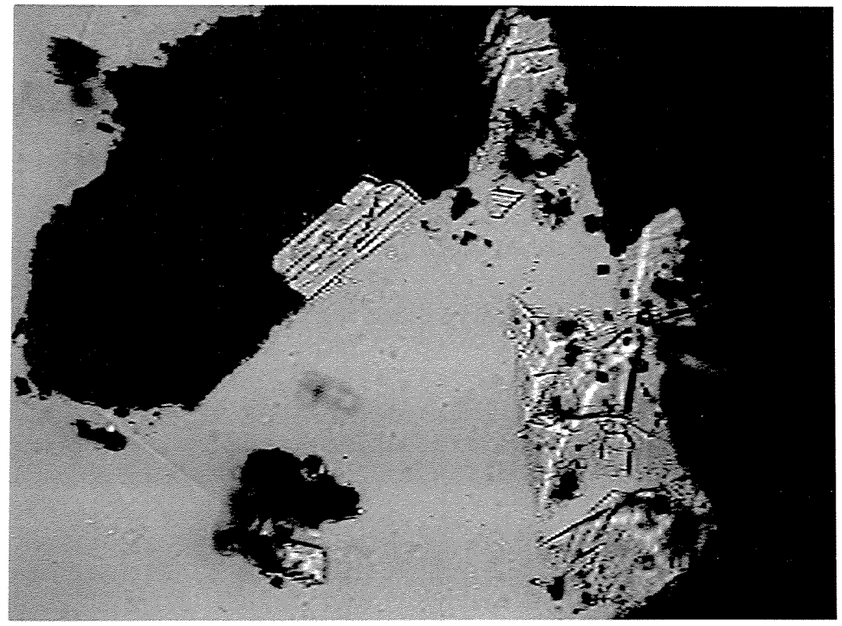

Figure 2b: *Anhydrite and polyhalite crystals in or adjacent to halite turned black (colloidal sodium) by the irradiation. Long edge = 0.2 mm; Nicols //*

The only way to obtain reliable information as to the amount of energy stored in the halite portion of the rock salt seemed to be to perform calorimetric measurements, be it on simple subsamples or on a halite concentrate separated by hand-picking under the microscope. Important in both cases is, that the calorimetric specimens have to be analyzed once more after they were measured, as the originally chosen composition can no longer be expected.

For a general information and evaluation of the potential role of trace elements both in the halite and the sulfate minerals of the rock salt an extensive description was given in the final report on 'Material inventory and petrophysics of the HAW-test field in the Asse' [Gies et al., 1994].

LITERATURE

A. GARCIA CELMA and H. DONKER, 1994: "*Radiation-Induced Creep of Confined NaCl*", Radiation Effects and Defects in Solids **132**, 223-247

H. GIES, H. GRESNER, H. HERBERT, N. JOCKWER, R. MITTELSTÄDT, J. MÖNIG, and F. NADLER, 1994: "*Material Inventory and Petrophysics of the Rock Salt in the HAW Field (Asse, 800-m-level)*", GSF-Report 16/94, Braunschweig, München, 186 p.

M. PAHL, 1988: "*Feinstratigraphische und mineralogisch-petrographische Aufnahme und Untersuchung der hangenden Horizonte des Staßfurt-Hauptsalzes im Bereich eines Versuchsfeldes zur Einlagerung hochradioaktiver Abfälle (HAW) auf der 800-m-mSohle der Schachtanlage Asse II bei Remlingen*".-Diplomarbeit. Geologisches Institut der TU Bausnchweig,

C.J. PEACH, 1991: "*Influence of Deformation on the Fluid Transport Properties of Rock Salts*", Ph.D. Thesis, Utrecht University, ISBN 90-71577-31-7.

C.J. PEACH, C.J. SPIERS, A.J. TANKINK, and H.J. ZWART, 1987: "*Fluid and Ionic Transport Properties of Deformed Salt Rock*", Commission of the European Communities, Nuclear Science and Technology Series, EUR 10926 EN, Brussels, Luxembourg, ISBN 92-825-6921-7.

C.J. SPIERS, C.J. PEACH, R.H. BRZESOWSKY, P.M.T.M. SCHUTJENS, J.L. LIEZENBERG, and H.J. ZWART, 1988: "*Long-Term Rheological and Transport Properties of Dry and Wet Salt Rocks*", Commission of the European Communities, Nuclear Science and Technology Series, EUR 11848 EN, Brussels, Luxembourg, ISBN 92-825-9191-3.

C.J. SPIERS, J.L. URAI, G.S. LISTER, J.N. BOLAND, and H.J. ZWART, 1986: "*The Influence of Fluid-Rock Interaction on the Rheology of Salt Rock*", Commission of the European Communities, Nuclear Science and Technology Series, EUR 10399 EN, Brussels, Luxembourg, 131 p.

J.L. URAI, C.J. SPIERS, H.J. ZWART, and G.S. LISTER, 1986: "*Weakening of Rock Salt by Water During Long-Term Creep*", Nature, **324**, 554 - 557.